

Data-driven sensitivity analysis in a total-reflection high-energy positron diffraction (TRHEPD) experiment of the $\text{Si}_4\text{O}_5\text{N}_3$ / 6H-SiC (0001)- $(\sqrt{3} \times \sqrt{3})$ R30° surface structure

Takeo Hoshi

Department of Applied Mathematics and Physics, Tottori University, 4-101
Koyama-Minami, Tottori 680-8550, Japan.
Advanced Mechanical and Electronic System Research Center, Faculty of
Engineering, Tottori University, 4-101 Koyama-Minami, Tottori 680-8550, Japan.

Daishiro Sakata

Department of Applied Mathematics and Physics, Tottori University, 4-101
Koyama-Minami, Tottori 680-8550, Japan.

Shotaro Oie

Department of Applied Quantum Physics and Nuclear Engineering, Kyushu
University, 744 Motooka, Nishi-ku, Fukuoka 819-0395, Japan

Izumi Mochizuki

Institute of Materials Structure Science, High Energy Accelerator Research
Organization (KEK), Oho 1-1, Tsukuba, Ibaraki, 305-0801, Japan

Satoru Tanaka

Department of Applied Quantum Physics and Nuclear Engineering, Kyushu
University, 744 Motooka, Nishi-ku, Fukuoka 819-0395, Japan

Toshio Hyodo

Institute of Materials Structure Science, High Energy Accelerator Research
Organization (KEK), Oho 1-1, Tsukuba, Ibaraki, 305-0801, Japan

Koji Hukushima

Graduate School of Arts and Sciences, The University of Tokyo 153-8902, Japan
Komaba Institute for Science, The University of Tokyo, 3-8-1 Komaba, Meguro,
Tokyo 153-8902, Japan

Abstract. The present article proposes a data analysis method for determining surface structures from experimental results, which consists of a non-linear optimization procedure and a sensitivity analysis. This method solves numerically the partial differential equation in the fully-dynamical quantum diffraction theory with many trial surface structures. In the sensitivity analysis, we focused on the experimental uncertainties and the variation over individual fitting parameters, which was analyzed by solving the eigenvalue problem of the variance-covariance matrix. A modern massively parallel supercomputer was used to complete the analysis within a moderate computational time. The sensitivity analysis provides a basis for the choice of variables in the data analysis for practical reliability. The significance of the present analysis method was demonstrated in the structure determination of a $\text{Si}_4\text{O}_5\text{N}_3$ / 6H-SiC(0001)- $(\sqrt{3} \times \sqrt{3})$ R30° surface in a total-reflection high-energy positron diffraction (TRHEPD) experiment.

1. Introduction

Data analysis procedures with practical reliability and moderate computational times are necessary features for measurement techniques in material science and other scientific fields. In general, the data analysis procedures determine target variables $X \equiv (X_1, X_2, \dots, X_n)$ from obtained experiment data, F_{exp} , for a chosen characteristic $F(X)$. The experimental data, F_{exp} , usually contains the uncertainty that stems from the measurement conditions and the apparatus, so it is desirable for a data analysis method also to provide some information on this associated uncertainty. Here we focus on the inverse problem in which the characteristic, F , can be calculated from physical theory as a forward problem with the function of the target variables X ($F_{\text{cal}} = F_{\text{cal}}(X)$). The data analysis is then reduced to the optimization process to minimize the residual difference $R(X)$ between the calculated characteristics, $F_{\text{cal}}(X)$, and the experimental data, F_{exp} ,

$$R = R(X) \equiv |F_{\text{cal}}(X) - F_{\text{exp}}|. \quad (1)$$

The function R is called the reliability factor or R-factor in certain physical fields.

Recently, we developed data analysis software with optimization process [1, 2] for total-reflection high-energy positron diffraction (TRHEPD) [3, 4, 5, 6, 7], a novel experimental probe for the accurate determination of surface structure. The target variable set X here are typically the atomic positions on the topmost surface layer and sub-surface layers below. Before the software was developed, the determination of X was performed by using a trial-and-error approach without a systematic optimization algorithm. In order to make the process more objective, we first developed an automatic optimization software for the surface atomic positions [1]. Then we proposed a two-stage optimization procedure [2], in which the first stage is a grid-based global search of the candidate regions in the X space where the absolutely optimized X could possibly exist, thus avoiding the possibility of ending up with a local optimization. The second stage is a local search for a final solution. In the present article, we apply the method proposed in Ref. [1] to the analysis of the surface structure of $\text{Si}_4\text{O}_5\text{N}_3 / 6\text{H-SiC} (0001) - (\sqrt{3} \times \sqrt{3}) \text{R}30^\circ$ [8, 9, 10], which consists of atoms to sub-nanometer depth. In addition, we propose a method of selecting an appropriate variable set X to which the experimental method is sensitive. This is useful since data analysis in a large data-space dimension, $n = \text{dim}(X)$, may impact on reliability and/or incur high computational cost.

The present paper is organized as follows: an overview of TRHEPD is described in Sec. 2; the present experiment is detailed in Sec. 3; the method and result of the data analysis are shown in Sec. 4; and a summary is given in Sec. 5.

2. Overview of TRHEPD

TRHEPD was first proposed in 1992 by Ichimiya [11] and realized in a study in 1998 by Kawasuso and Okada [12]. Following a period of initial development by the Kawasuso group, this technique has been actively developed in the last decade at the Slow Positron

Facility (SPF), Institute of Materials Structure Science (IMSS), High Energy Accelerator Research Organization (KEK) [3, 4, 5, 6, 7]. Since the volume fraction of the surface region is much smaller than that of the bulk region, the experimental probe should be sensitively selective to the atoms in the surface region. While the experimental setup of TRHEPD is essentially the same as that for reflection high-energy electron diffraction (RHEED), TRHEPD has a higher surface sensitivity than RHEED due to a particular physical property of materials - since the electrostatic potential in every material is positive, the potential energy of the positron in the material is positive while that of the electron is negative. Thus, the positron probes more selectively the topmost and sub-surface atomic layers, which makes the positron an ideal probe of surface structure. In fact, the probing depth of the positron is on the sub-nanometer order, as shown through a model calculation in Fig. 3 of Ref. [4], which leads to the surface selectivity of TRHEPD and RHEED being remarkably different in the lower incident glancing-angle region.

The purpose of the TRHEPD data analysis is to determine the surface structure X or a set of the atomic positions (X_1, X_2, \dots, X_n) on the topmost and sub-surface layers below. The expected diffraction characteristics from the atomic arrangements in the surface region and a semi-infinite bulk region, called a rocking curve, is calculated as a function of the surface structure ($F_{\text{cal}} \equiv F_{\text{cal}}(X)$), like that in RHEED, by solving the partial differential equation in a fully-dynamical quantum diffraction theory [13, 14]. In the previous paper [2], we used the diffraction data of Ge(001)-c(4 × 2) surface generated numerically by the partial differential equation, instead of real experimental data. The present article reports the analysis of real experimental data with the additional sensitivity analysis.

3. Experiment

3.1. Material

The surface measured by TRHEPD in the present work is $\text{Si}_4\text{O}_5\text{N}_3 / 6\text{H-SiC}$ (0001)- $(\sqrt{3} \times \sqrt{3})$ R30° [8, 9, 10]. Figure 1 shows a side view of the structure reported in references [8, 9, 10]. The z axis is chosen to be perpendicular to the surface. The top view is found, for example, in Fig.1(c) of Ref.[10]. We restricted ourselves to the analysis of the TRHEPD data in the one-beam condition (See Sec. 3.2) which is sensitive only to the atomic coordinates perpendicular to the surface, z . The notation of the atomic sites in Fig. 1, such as O1, Si1 and O2, follows that in Ref. [10]. The z coordinates of the sites are denoted as $z_1(\text{O1})$, $z_2(\text{Si1})$, $z_3(\text{O2})$, $z_4(\text{Si2})$, $z_5(\text{N})$, $z_6(\text{Si3})$, $z_7(\text{C1})$, $z_8(\text{C2})$, $z_9(\text{Si4})$, $z_{10}(\text{Si5})$, and $z_{11}(\text{C3})$ in the descending order ($z_1 > z_2 > \dots > z_{11}$).

The preparation of the sample (of size $5 \times 10 \text{ mm}^2$) was as follows. The epitaxial SiON layer was grown on an on-axis 4H-SiC(0001) substrate [8]. The substrate was initially etched by hydrogen gas under atmospheric pressure at 1623K for 15 min to clean and atomically smoothen the surface [15], and subsequently exposed to nitrogen

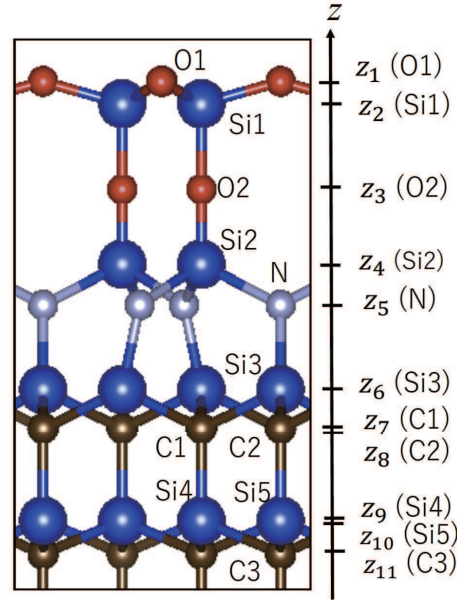


Figure 1. Side view of the surface structure of Si₄O₅N₃ / 6H-SiC (0001)-(√3 × √3) R30° [8, 9, 10].

gas at the same temperature. Oxygen gas was not intentionally introduced in this experiment but may have been mixed in the reactant as an impurity and/or through small leaks. Samples were then transferred to the TRHEPD measurement chamber and further annealed (973 K, 60 min) in UHV (less than 1.0×10^{-7} Pa) to remove surface contamination.

3.2. TRHEPD measurement

The overview and details of the TRHEPD station at the KEK-IMSS-SPF are described elsewhere [6, 16, 17]. A linac-based brightness-enhanced positron beam with an energy of 10 keV was used. The diffraction patterns were obtained under the one-beam condition [14, 4], where the beam azimuthal angle was set at 7.5° off the $[11\bar{2}0]$ direction. In this condition the diffraction spot intensity depends primarily on the atomic coordinates perpendicular to the surface because the in-plane diffraction is effectively suppressed. The dependence of the 00-spot diffraction intensity ($I_{00}^{(\text{exp})}(\theta)$) on the glancing angle (θ) of incidence, called the rocking curve [14, 4], was extracted from the series of TRHEPD patterns, taken with an exposure time of 1.5 min each. The glancing angle was varied from $\theta_{\min} = 0.5^\circ$ to $\theta_{\max} = 6.5^\circ$ in $\Delta\theta = 0.1^\circ$ steps by rotating the sample. The experimental rocking curve was expressed as $F_{\text{exp}} = (I_{00}^{(\text{exp})}(\theta_1 = \theta_{\min}), \dots, I_{00}^{(\text{exp})}(\theta_\nu = \theta_{\max}))$, with $\nu \equiv 1 + (\theta_{\max} - \theta_{\min})/\Delta\theta = 61$. The experimental data and the corresponding calculated values were normalized ($|F_{\text{exp}}| = \{\sum_i^\nu |I_{00}^{(\text{exp})}(\theta_i)|^2\}^{1/2} = 1$ and $|F_{\text{cal}}| = \{\sum_i^\nu |I_{00}^{(\text{cal})}(\theta_i)|^2\}^{1/2} = 1$, respectively), when the R-factor (1) was calculated. Since only the data obtained in the one-beam condition were analyzed, the procedure described in the next subsection concerns only

that with the z coordinates ($X = (z_1, z_2, \dots)$).

4. Data analysis

The present data analysis consists of the optimization procedure described in Refs. [1, 2] and the sensitivity analysis. Among existing papers of TRHEPD [4], the structure X is accepted as a final solution when the R-factor (R) is optimized to be less than 0.02 ($R(X) \leq 0.02$).

In the analysis, the coordinate z_{11} is set to be the origin ($z_{11} \equiv 0$). The atomic positions at the deeper layers ($z < z_{11}$) is set to that in the bulk. The initial z coordinates were chosen to be equivalent to those in Table I of Ref. [10]; $(z_1, z_2, z_3, z_4, z_5, z_6, z_7, z_8, z_9, z_{10}) = (z_1^{(\text{ini})}, z_2^{(\text{ini})}, z_3^{(\text{ini})}, z_4^{(\text{ini})}, z_5^{(\text{ini})}, z_6^{(\text{ini})}, z_7^{(\text{ini})}, z_8^{(\text{ini})}, z_9^{(\text{ini})}, z_{10}^{(\text{ini})}) = (9.19\text{\AA}, 8.67\text{\AA}, 7.04\text{\AA}, 5.45\text{\AA}, 4.83\text{\AA}, 3.11\text{\AA}, 2.63\text{\AA}, 2.44\text{\AA}, 0.67\text{\AA}, 0.59\text{\AA})$. The present calculations were carried out by the supercomputer Oakforest-PACS with Intel Xeon PhiTM 7250 processors. The use of the supercomputer was crucial only in the sensitivity analysis, since the optimization analysis consumes only a tiny computational cost. The calculated rocking curve, $F_{\text{cal}} = F_{\text{cal}}(X)$, was generated by the solver routine of the fully-dynamical quantum diffraction theory used in Ref. [18], as in our previous works [1, 2].

4.1. Optimization analysis with eight variables

First, the eight coordinates ($z_1, z_2, z_3, z_4, z_5, z_6, z_7, z_8$) were chosen to be the variables in the optimization procedure ($R = R(z_1, z_2, z_3, z_4, z_5, z_6, z_7, z_8)$), which consist of the whole SiON region (z_1, z_2, z_3, z_4, z_5) and a set of bulk SiC layers (z_6, z_7, z_8). The variables z_9, \dots, z_{11} are fixed to be those in the initial structure. The calculated system contains a semi-infinite bulk region, as in the existing papers of TRHEPD measurement [4].

The iterative optimization analysis was made using the gradient-free, Nelder-Mead algorithm [19, 20]. A Python code was developed for this purpose by some of the present authors [1, 2]. The Nelder-Mead algorithm was performed by a module in the scipy library (scipy.optimize.fmin). Hereafter we use the notation X for the vector $X = (z_1, z_2, z_3, z_4, z_5, z_6, z_7, z_8)^T$ in the eight-dimensional data space. In the Nelder-Mead algorithm, some of the set of $n + 1 (= 9)$ sampling points $\{X^{(l)}\}^{[k]} (l = 0, 1, \dots, 8)$ are replaced by new points suitably found by calculation in every iteration, where l is the sampling point index and k is the iteration step index ($k = 0, 1, 2, \dots$). The best sampling point $X^{[k]} \equiv \text{argmin}_l(\{R(X^{(l)})\}^{[k]})$ is obtained in the course of the iteration. The iterative procedure is performed until the R-factor value converges within a given convergence criteria of $\Delta R = 0.05 \times 10^{-2}$. The initial data of the sampling points $\{X^{(l)}\}^{[k]} (l = 0, 1, 2, \dots, 8)$ is chosen by the researcher. The structure in Ref. [10] was chosen to be the initial data of the zero-th sampling point $X^{0} = (z_1^{0}, z_2^{0}, \dots, z_8^{0})^T$, as mentioned above. The initial data of the other sampling points $\{X^{(l)}\}^{[0]} (l = 1, 2, \dots, 8)$ were chosen so that the l -th sampling point

$X^{(l)[0]} = (z_1^{(l)[0]}, z_2^{(l)[0]}, \dots, z_8^{(l)[0]})^T$ is displaced by 0.05 \AA from the zero-th sampling point X^{0} only in the l -th coordinate ($z_l^{(l)[0]} = z_l^{(0)[0]} + 0.05 \text{ \AA}$, $z_i^{(l)[0]} = z_i^{0}$ for $i \neq l$).

The optimization process with the Nelder-Mead algorithm converged at the 42-th iteration. This took the computational time, T , of approximately 1.0 minutes of one CPU of the Oakforest-PACS. The R-factor values for the initial and converged structures were $R^{(\text{ini})} = R(X^{(\text{ini})}) = 2.28 \times 10^{-2}$ and $R^* = R(X^*) = 0.91 \times 10^{-2}$, respectively. The converged point was $X^* = (z_1^*, z_2^*, \dots, z_8^*) \approx (9.09 \text{ \AA}, 8.67 \text{ \AA}, 7.03 \text{ \AA}, 5.60 \text{ \AA}, 4.80 \text{ \AA}, 3.11 \text{ \AA}, 2.64 \text{ \AA}, 2.44 \text{ \AA})$. The difference between the initial and converged structures ($\delta z_i \equiv z_i^* - z_i^{(\text{ini})}$) was $(\delta z_1, \delta z_2, \delta z_3, \delta z_4, \delta z_5, \delta z_6, \delta z_7, \delta z_8) \approx (-0.10 \text{ \AA}, 0.00 \text{ \AA}, -0.01 \text{ \AA}, 0.15 \text{ \AA}, -0.03 \text{ \AA}, 0.00 \text{ \AA}, 0.01 \text{ \AA}, 0.00 \text{ \AA})$.

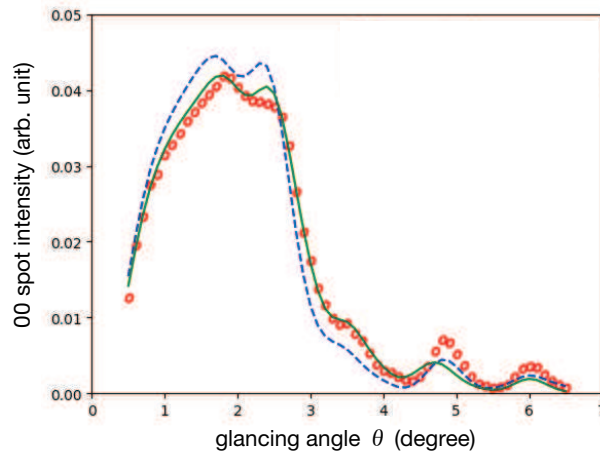


Figure 2. Comparison of the experimental rocking curve (open circles), the calculated values for the initial structure (dashed line) and the calculated values for the converged structure (solid line) in the eight-variable optimization.

Figure 2 shows the calculated rocking curves F_{cal} in the initial and converged structures and the experimental data F_{exp} . The calculated rocking curves F_{cal} in the converged structure agrees with the experimental data F_{exp} more closely than that in the initial structure but the two calculated structures show only small difference ($|\delta z_i| \leq 0.15 \text{ \AA}$). This exhibits the sensitivity of TRHEPD technique. While it is certain that the structure of the present specimen is essentially the same as that in the previous papers [8, 9, 10], it would be of interest to see whether the difference in the sample preparation procedure produced this small difference.

4.2. Sensitivity analysis

The sensitivity analysis was carried out after the optimization, by capturing the numerical behavior of $R(X)$ near the converged point X^* . We used supercomputers to compute $R(X)$ on the local grid of the coordinates $z_i \equiv z_i^* + mh$ for $m = -3, -2, -1, 0, 1, 2, 3$ and $i = 1, \dots, 8$ with the uniform grid interval $h = 0.05 \text{ \AA}$. The total number of eight-dimensional grid points was $N_{\text{grid}} = 7^8 = 5,764,801$. Although the total

operational cost on the grid points is large, a fast computation is possible on modern massive parallel supercomputers. The parallelism was carried out with Message Passing Interface (MPI) and each CPU executed one MPI process. The total computational time T with the N_{grid} grid points was approximately 1.5 hours using $N_{\text{CPU}} = 2,048$ CPUs of Oakforest-PACS. Each CPU calculated the R-factor $R(X)$ at approximately $N_{\text{grid}}/N_{\text{CPU}} \approx 2815$ grid points.

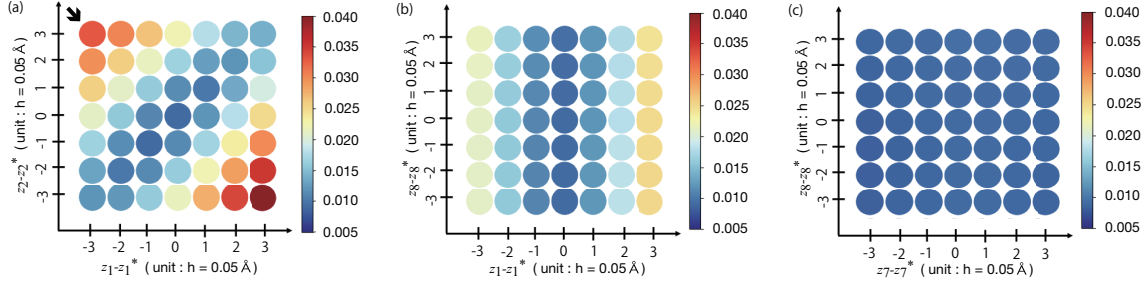


Figure 3. (a) The color-coded isovalue plots of $R(X)$ on the local grid of the z_1 - z_2 plane. The $(1, -1, 0, 0, 0, 0, 0, 0)^T$ direction is depicted as the bold arrow located at the left upper corner. (b) The color-coded isovalue plots on the local grid of the z_1 - z_8 plane. (c) The color-coded isovalue plots on the local grid of the z_7 - z_8 plane. The difference between the maximum and minimum values of $R(X)$ among the plotted grid points is less than 0.1 in (c).

Figure 3 demonstrates the anisotropic sensitivity among a few two-dimensional isovalue plots of $R = R(z_1, z_2, \dots, z_8)$ on the local grid with the use of color-coding. Figure 3(a) is the isovalue plot on the z_1 - z_2 plane, where all the other variables are fixed to be the converged values ($z_i = z_i^*$ for $i = 3-8$). We found that the function $R(X)$ is quite sensitive to the deviation in the $(1, -1, 0, 0, 0, 0, 0, 0)^T$ direction, showing that the diffraction signal was contributed to significantly by the interaction of the positron waves scattered from the two atomic layers at z_1 and z_2 , and is sensitive to the difference of the two atomic layers ($z_1 - z_2$). Figure 3(b) is the isovalue plot on the z_1 - z_8 plane showing that the function $R(X)$ is insensitive to the deviation in the $(0, 0, 0, 0, 0, 0, 0, 1)^T$ direction or the z_8 -axis direction. Figure 3(c) is the isovalue plot on the z_7 - z_8 plane and indicates that the function $R(X)$ is insensitive to any deviation on the z_7 - z_8 plane. These properties are consistent with surface selectivity or the statement that the TRHEPD measurement probes mainly the shallow region with $z \geq z_6$. We should note, however, that Figure 3 depicts the numerical behavior of $R(X)$ only within a partial space of the eight-dimensional data space.

The anisotropic behavior of the function $R(X)$ on the whole data space was represented by the variance-covariance matrix S , whose (i, j) component is defined as

$$S_{ij} \equiv \frac{1}{\Omega} \int (z_i - z_i^*)(z_j - z_j^*)W(X)dX \quad (2)$$

for $i, j = 1, 2, \dots, 8$ with the weight function

$$W(X) \equiv e^{-(R(X)-R^*)/s} \quad (3)$$

and the normalization factor

$$\Omega \equiv \int W(X)dX. \quad (4)$$

A parameter $s = 0.002$, called the scaling parameter, is introduced, which is the tolerance measure of the uncertainty for the R-factor value. It is noteworthy that the function $R(X)$ can be written formally by the second-order Taylor expansion

$$R(X)/s \approx R(X^*)/s + \sum_{i,j}^n (z_i - z_i^*)\Gamma_{ij}(z_j - z_j^*), \quad (5)$$

with $\Gamma_{ij} \equiv \partial^2(Rs^{-1})/(\partial z_i \partial z_j)$ of the curvature matrix Γ . If the third- and higher-order terms of the Taylor expansion are ignored, the inverse matrix of S is the curvature matrix Γ ($S = \Gamma^{-1}$). The iso-value plot of Eq. (5) ($R(X) = (\text{constant})$) forms an n -dimensional ellipsoid and the k -th eigenvector \mathbf{v}_k indicates a principal axis of the n -dimensional ellipsoid.

When the integrals in Eq. (2) and Eq. (4) are reduced to the sum over the local grid points defined at the beginning of this section, the matrix S was obtained as

$$S \approx \begin{pmatrix} 7.39 & 6.59 & 3.38 & 3.20 & 0.43 & -0.02 & 0.04 & 0.19 \\ & 7.52 & 3.18 & 2.58 & 1.30 & 0.33 & -0.47 & 0.12 \\ & & 8.18 & 1.07 & 0.23 & 0.53 & 0.02 & 0.08 \\ & & & 7.59 & 2.04 & 1.41 & -0.40 & 0.13 \\ & & & & 9.02 & 0.63 & -0.05 & 0.17 \\ & & & & & 8.93 & -1.06 & 0.05 \\ & & & & & & 10.66 & 0.01 \\ & & & & & & & 9.87 \end{pmatrix} \quad (6)$$

in units of 10^{-3} \AA^2 . The matrix, S , is symmetric and Eq. (6) shows only the upper triangular elements explicitly. The importance of the off-diagonal elements is characterized by the quantity $q_i \equiv (\sum_{j \neq i} |S_{ij}|)/|S_{ii}|$ for each column ($i = 1, 2, \dots, 8$). The values were $q_1 = 1.87, q_2 = 1.94, q_3 = 1.04, q_4 = 1.43, q_5 = 0.54, q_6 = 0.45, q_7 = 0.19, q_8 = 0.08$. It was found that the off-diagonal elements are significant among the first to fifth columns ($q_i \geq 0.5$ for $i = 1, \dots, 5$). The presence of the significant off-diagonal elements in S indicates that the effect of the displacement of each atomic layer correlates significantly to the value of the R-factor in the first to fifth layers.

The principal deviation direction in the eight-dimensional data space is obtained by solving the 8×8 matrix eigenvalue equation

$$S\mathbf{v}_k = \lambda_k \mathbf{v}_k \quad (7)$$

with $0 \leq \lambda_1 \leq \lambda_2 \leq \dots \leq \lambda_8$ and $|\mathbf{v}_k| = 1$. The k -th eigenvalue λ_k indicates the directional variance in the \mathbf{v}_k direction. The values were $\lambda_1 = 0.73 \times 10^{-3} \text{ \AA}^2$, $\lambda_2 = 4.53 \times 10^{-3} \text{ \AA}^2$, $\lambda_3 = 6.18 \times 10^{-3} \text{ \AA}^2$, $\lambda_4 = 8.20 \times 10^{-3} \text{ \AA}^2$, $\lambda_5 = 9.62 \times 10^{-3} \text{ \AA}^2$,

$\lambda_6 = 9.92 \times 10^{-3} \text{Å}^2$, $\lambda_7 = 11.3 \times 10^{-3} \text{Å}^2$, $\lambda_8 = 18.7 \times 10^{-3} \text{Å}^2$. The sum of the eigenvalues $\text{Tr}[S] = \sum_{k=1}^8 \lambda_k$ quantifies the total uncertainty and the difference between the eigenvalues indicates the anisotropy in the uncertainty. For example, the first eigenvector \mathbf{v}_1 with the smallest eigenvalue (directional variance) λ_1 represents the most sensitive direction or the direction with the smallest uncertainty.

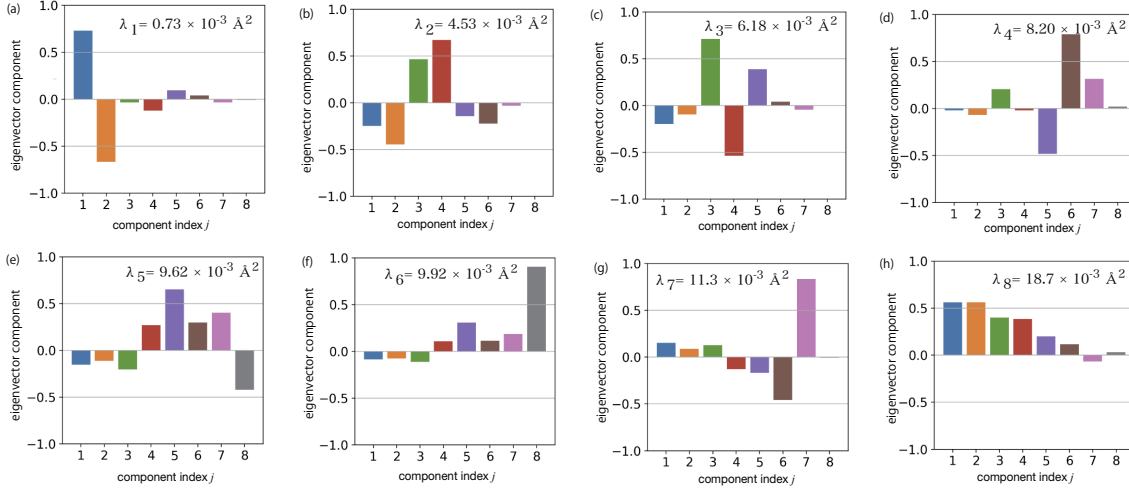


Figure 4. The components of the eigenvectors $\mathbf{v}_k = (v_{1k}, v_{2k}, \dots, v_{8k})^T$ for (a) $k = 1$, (b) $k = 2$, (c) $k = 3$, (d) $k = 4$, (e) $k = 5$, (f) $k = 6$, (g) $k = 7$, (h) $k = 8$. The values of the eigenvalues (directional variance) λ_k ($k = 1, 2, \dots, 8$) are given in each graph.

Figure 4 shows the values of the eigenvector components $\mathbf{v}_k = (v_{1k}, v_{2k}, \dots, v_{8k})^T$ for $k = 1, 2, \dots, 8$ revealing the principal axis directions for the anisotropic sensitivity. As an example, the first eigenvector \mathbf{v}_1 is approximated to be $\mathbf{v}_1 \approx (1/\sqrt{2})(1, -1, 0, 0, 0, 0, 0, 0)^T$ and thus the function $R(X)$ should be quite sensitive to the deviation in the $(1, -1, 0, 0, 0, 0, 0, 0)^T$, as seen on Figure 3(a). As another example, the sixth and seventh eigenvectors are similar to the eighth and seventh original axis vectors ($\mathbf{v}_6 \approx (0, 0, 0, 0, 0, 0, 0, 1)^T$, $\mathbf{v}_7 \approx (0, 0, 0, 0, 0, 0, 1, 0)^T$), respectively, which indicates that almost no interacting wavefunction is formed by the scattering process at the seventh and eighth atomic layers and so the variables z_7 and z_8 are hardly correlated to the other variables. Thus the function $R(X)$ may be almost unchanged on the (z_7, z_8) plane, as seen on Figure 3(c). In addition, it is also noted that $\mathbf{v}_8 \approx (1/\sqrt{5})(1, 1, 1, 1, 1, 0, 0, 0)^T$ in Figure 4(h), which means that the function $R(X)$ is hardly affected by the constant shift among z_1, z_2, z_3, z_4 and z_5 ($z_i \Rightarrow z_i + \alpha$ for $i = 1, \dots, 5$). In other words, the function $R(X)$ is contributed mainly by the relative positions between the atoms within the slab region that contains the first to fifth layers.

4.3. Optimization analysis with six variables

The above sensitivity analysis implies that the optimization analysis with the six variables $(z_1, z_2, z_3, z_4, z_5, z_6)$ would give a reasonable result. Thus, we performed

the optimization analysis with these six variables. The calculated system is a slab that consists only of the eleven layers at $z = z_1, \dots, z_{11}$ in Figure 1, neglecting the bulk part, since the R-factor should hardly be sensitive to an atomic positions of deeper layers ($z < z_{11}$). The variables $z_7, z_8, z_9, z_{10}, z_{11}$ are fixed to be those in the initial structure.

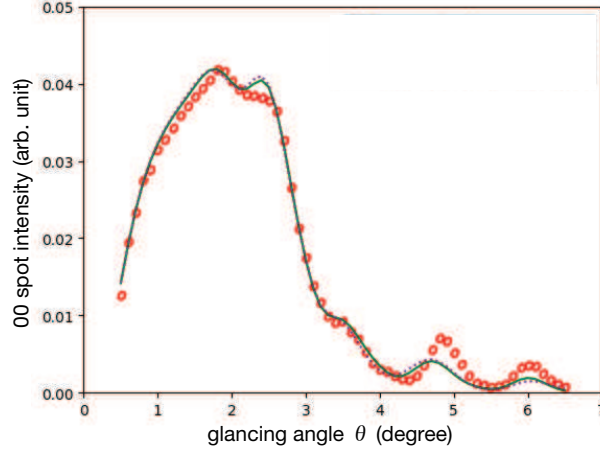


Figure 5. Comparison of the experimental rocking curve (open circles), the calculated values for the converged structure in the eight-variable optimization (solid line) and the calculated values for the converged structure in the six-variable optimization (dotted line).

The iterative optimization process was converged at the 32-nd iteration step. The converged point was $X^* = (z_1^*, z_2^*, \dots, z_6^*) \approx (9.12 \text{ \AA}, 8.69 \text{ \AA}, 7.08 \text{ \AA}, 5.58 \text{ \AA}, 4.76 \text{ \AA}, 3.09 \text{ \AA})$. The R-factor value at the converged structure was $R^* = R(X^*) = 0.97 \times 10^{-2}$. The difference in the initial and converged structure ($\delta z_i \equiv z_i^* - z_i^{(\text{ini})}$) was $(\delta z_1, \delta z_2, \delta z_3, \delta z_4, \delta z_5, \delta z_6) \approx (-0.07 \text{ \AA}, 0.02 \text{ \AA}, 0.04 \text{ \AA}, 0.13 \text{ \AA}, -0.07 \text{ \AA}, -0.02 \text{ \AA})$. The difference in the converged coordinates between the eight- and six-variable analyses was $(-0.03 \text{ \AA}, -0.02 \text{ \AA}, -0.05 \text{ \AA}, 0.02 \text{ \AA}, 0.04 \text{ \AA}, 0.02 \text{ \AA})$ for $(z_1^*, z_2^*, \dots, z_6^*)$. Figure 5 shows the calculated rocking curves in the converged structures by the eight- and six-variable optimization procedure and the experimental data. Since the eight- and six-variable optimization procedures gives only a small difference between the resulting converged structure and the rocking curves, we concluded that both optimization procedures are acceptable.

The present sensitivity analysis gives a guide for the practical choice of a set of variables acceptable both in computational cost and reliability.

4.4. Generality of sensitivity analysis

Finally, we comment on the generality of the above data-driven sensitivity analysis. The sensitivity analysis gives a foundation for the appropriate choice of the variable set X by solving the eigenvalue equation of the variance-covariance matrix. For example, if a material contains light and heavy atoms, the TRHEPD diffraction signal tends to be more sensitive to a heavy atom than to a light atom. For such cases, it is not

trivial to choose a proper set of variables because a heavy atom at a deeper layer may make a larger contribution to the diffraction signal than a light atom at a shallower layer. Moreover, the analysis method is applicable to more general cases, since it can handle variables of different physical dimension at the same time, such as the position and the coverage (occupation fraction) of each surface atom. We hope to apply the method to other diffraction experiments for two-dimensional structures, such as surface X-ray diffraction (SXR), low energy electron diffraction (LEED), low energy positron diffraction (LEPD) [21, 22] and other experiments.

It should be noted that a grid-based calculation may incur a high computational cost with the large data dimension. In such a case, the Monte Carlo sampling method is promising both in the optimization procedure and the numerical integration such as Eq. (2). There are already research examples [23, 24] in which the Monte Carlo method has been used for the analysis of SXR data, though the sensitivity analysis with the eigenvalue problem in Eq. (7) was not performed. Furthermore, it would be desirable to utilize the parallelizable Monte Carlo method [25] that can efficiently use massively parallel supercomputers.

5. Summary

The present article proposes a data-driven sensitivity analysis method. The method is based on the eigenvalue problem with the variance-covariance matrix and forms a foundation for an appropriate choice of the variables in the data analysis with practical reliability and moderate computational time. The analysis was applied to the total-reflection high-energy positron diffraction (TRHEPD) experiment for the surface structure determination of $\text{Si}_4\text{O}_5\text{N}_3 / 6\text{H-SiC} (0001) - (\sqrt{3} \times \sqrt{3}) \text{R}30^\circ$. The data-driven analysis confirms the high surface sensitivity of TRHEPD for the topmost and sub-surface atomic layers to sub-nanometer depths. The method is general and may be applied in wide range of experimental techniques.

Acknowledgement

The present research is supported partly by the Grant-in-Aid for Scientific Research (KAKENHI) from Japan Society for the Promotion of Science (19H04125, 19K12634 and 20H00581) and by the Ministry of Education, Culture, Sports, Science and Technology (MEXT) of Japan as a subgroup of 'Social and scientific priority issue (Creation of new functional devices and high-performance materials to support next-generation industries; CDMSI) to be tackled by using post-K computer'. Numerical computations were carried out by the supercomputer Oakforest-PACS for Interdisciplinary Computational Science Program in the Center for Computational Sciences, University of Tsukuba and the Joint Usage/Research Center for Interdisciplinary Large-scale Information Infrastructures (Project ID: jh200045-NAH). The numerical computation was carried out also at the Supercomputer Center, Institute for Solid State Physics,

University of Tokyo and at the Academic Center for Computing and Media Studies, Kyoto University. We thank Kazuyuki Tanaka and Takashi Hanada for fruitful discussions on the code.

- [1] K. Tanaka, T. Hoshi, I. Mochizuki, T. Hanada, A. Ichimiya, and T. Hyodo. *Acta. Phys. Pol. A*, 137:188, 2020.
- [2] K. Tanaka, I. Mochizuki, T. Hanada, A. Ichimiya, T. Hyodo, and T. Hoshi. JJAP Conf. Series, in press; Preprint:<https://arxiv.org/abs/2002.12165/>.
- [3] C. Hugenschmidt. *Surf. Sci. Rep.*, 71:547, 2016.
- [4] Y. Fukaya, A. Kawasuso, A. Ichimiya, and T. Hyodo. *J. Phys. D*, 52:013002, 2019.
- [5] Y. Fukaya. Chapter 4 - Diffraction: Determination of atomic structure. In I. Matsuda, editor, *Monatomic Two-Dimensional Layers*, Micro and Nano Technologies, pages 75 – 111. Elsevier, 2019.
- [6] I. Mochizuki, H. Ariga, Y. Fukaya, K. Wada, M. Maekawa, A. Kawasuso, T. Shidara, K. Asakura, and T. Hyodo. *Phys. Chem. Chem. Phys.*, 18:7085, 2016.
- [7] Y. Endo, Y. Fukaya, I. Mochizuki, A. Takayama, T. Hyodo, and S. Hasegawa. *Carbon*, 157:857, 2020.
- [8] T. Shirasawa, K. Hayashi, S. Mizuno, S. Tanaka, K. Nakatsuji, F. Komori, and H. Tochiyama. *Phys. Rev. Lett.*, 98:136105, 2007.
- [9] T. Shirasawa, K. Hayashi, H. Yoshida, S. Mizuno, S. Tanaka, T. Muro, Y. Tamenori, Y. Harada, T. Tokushima, Y. Horikawa, E. Kobayashi, T. Kinoshita, S. Shin, T. Takahashi, Y. Ando, K. Akagi, S. Tsuneyuki, and H. Tochiyama. *Phys. Rev. B*, 79:241301, 2009.
- [10] S. Mizuno, T. Matsuo, and T. Nakagawa. *Surf. Sci.*, 661:22, 2017.
- [11] A. Ichimiya. In *Positrons at Metallic Surfaces*, volume 28 of *Solid State Phenomena*, pages 143–148. Trans Tech Publications Ltd, 1992.
- [12] A. Kawasuso and S. Okada. *Phys. Rev. Lett.*, 81:2695, 1998.
- [13] A. Ichimiya. *Jpn. J. Appl. Phys.*, 22:176, 1983.
- [14] A. Ichimiya. *Surf. Sci. Lett.*, 192:L893, 1987.
- [15] H. Nakagawa, S. Tanaka, and I. Suemune. *Phys. Rev. Lett.*, 91:226107, 2003.
- [16] K. Wada, T. Hyodo, A. Yagishita, M. Ikeda, S. Ohsawa, T. Shidara, K. Michishio, T. Tachibana, Y. Nagashima, Y. Fukaya, M. Maekawa, and A. Kawasuso. *Eur. Phys. J. D*, 66:37, 2012.
- [17] M. Maekawa, K. Wada, Y. Fukaya, A. Kawasuso, I. Mochizuki, T. Shidara, and T. Hyodo. *Eur. Phys. J. D*, 68:165, 2014.
- [18] T. Hanada, H. Daimon, and S. Ino. *Phys. Rev. B*, 51:13320, 1995.
- [19] J. A. Nelder and R. Mead. *The Computer Journal*, 7:308, 1965.
- [20] M. Wright. Direct search methods: Once scorned, now respectable. In DF Griffiths and GA Watson, editors, *Numerical analysis*, pages 191–208. Addison-Wesley, 1996.
- [21] S. Y. Tong. *Surf. Sci.*, 457:L432, 2000.
- [22] K. Wada, T. Shirasawa, I. Mochizuki, M. Fujinami, M. Maekawa, A. Kawasuso, T. Takahashi, and T. Hyodo. *e-J. Surf. Sci. Nanotechnol.*, 16:313, 2018.
- [23] M. Anada, Y. Nakanishi-Ohno, M. Okada, T. Kimura, and Y. Wakabayashi. *J. Appl. Cryst.*, 50:1611, 2017.
- [24] M. Anada, K. Kowa, H. Maeda, E. Sakai, M. Kitamura, H. Kumigashira, O. Sakata, Y. Nakanishi-Ohno, M. Okada, T. Kimura, and Y. Wakabayashi. *Phys. Rev. B*, 98:014105, 2018.
- [25] K. Hukushima and Y. Iba. *AIP Conf. Proc.*, 690:200, 2003.